Analysis on error of laser frequency locking for fiber optical receiver in direct detection wind lidar based on Fabry–Perot interferometer and improvements

Feifei Zhang,[a,b] Xiankang Dou,[a,b] Dongsong Sun,[a,b] Zhifeng Shu,[a,b,*] Haiyun Xia,[a,b] Yuanyuan Gao,[a,b] Dongdong Hu,[a,b] and Mingjia Shangguan[a,b]
[a]Chinese Academy of Science, Key Laboratory of Geospace Environment, No. 96, Jinzhhai Road, Baohe District, Hefei 230026, China
[b]University of Science and Technology of China, School of Earth and Space Science, No. 96, Jinzhhai Road, Baohe District, Hefei 230026, China

Abstract. Direct detection Doppler wind lidar (DWL) has been demonstrated for its capability of atmospheric wind detection ranging from the troposphere to stratosphere with high temporal and spatial resolution. We design and describe a fiber-based optical receiver for direct detection DWL. Then the locking error of the relative laser frequency is analyzed and the dependent variables turn out to be the relative error of the calibrated constant and the slope of the transmission function. For high accuracy measurement of the calibrated constant for a fiber-based system, an integrating sphere is employed for its uniform scattering. What is more, the feature of temporally widening the pulse laser allows more samples be acquired for the analog-to-digital card of the same sampling rate. The result shows a relative error of 0.7% for a calibrated constant. For the latter, a new improved locking filter for a Fabry–Perot Interferometer was considered and designed with a larger slope. With these two strategies, the locking error for the relative laser frequency is calculated to be about 3 MHz, which is equivalent to a radial velocity of about 0.53 m/s and demonstrates the effective improvements of frequency locking for a robust DWL. [DOI: 10.1117/1.OE.53.12.124102]

Keywords: wind; lidar; Fabry–Perot interferometer; edge technique; frequency locking.

Paper 141327 received Aug. 26, 2014; accepted for publication Oct. 24, 2014; published online Dec. 2, 2014.

1 Introduction

Wind measurements are fundamental for understanding the dynamical and thermal processes in the atmosphere.[1] Doppler wind lidar (DWL) is now considered as an efficient method for wind measurements. More specially, direct detection lidar, utilizing Fabry–Perot interferometer (FPI) as a frequency discriminator, has been demonstrated for its ability of wind detection ranging from the troposphere to stratosphere in several missions by the National Aeronautics and Space Administration (NASA) and European Space Agency (ESA).[2–4]

The lidar systems using direct detection techniques, namely a double-edge technique, have been developed and reported by a number of researchers.[5–8] These systems perform by measuring the Doppler shift between atmospheric backscatter and the transmitted laser. However, the laser frequency, which is the reference frequency for Doppler shift, is jittering and drifting throughout the process, and an extra locking channel is added to trace the laser frequency for the FPI. Therefore, the locking accuracy should be ensured to maintain the accuracy of this relative Doppler shift.

Based on the former DWL system,[8,9] a new lidar was developed and the results are reported.[10] The optical receiver is upgraded to an all fiber-based system for compactness and easy optical adjustment, which will also benefit airborne and space-borne DWL.

In this paper, the frequency locking accuracy will be discussed and the problems caused by a fiber device in the optical receiver will be analyzed. After analysis, the improvements of the locking channel for this fiber-based receiver and the related results are presented.

2 Analysis

2.1 *Optical Receiver Description*

The basic principle of the double-edge technique for radial wind measurement by Rayleigh DWL has been described in detail elsewhere.[5,7] Here, it will be briefly reviewed, as illustrated in Fig. 1. The pulse laser is transmitted and backscattered by aerosols and molecules, and the spectrum of backscatters is presented by the dash dot line in Fig. 1. The received signal, spectrally broadened by thermal agitation of the atmospheric molecules and Doppler shifted by macroscale atmospheric motion which is called wind, is spectrally analyzed by a triple-channel cavity tunable FPI.

With a slightly different spacing among the three areas on the plate of the FPI, two edge filters and an extra locking filter are produced. By comparison of the fluxes transmitted through both edge filters, the radial Doppler shift that contains the laser and FPI jitter induced frequency shift is retrieved. From the laser frequency locking channel, this induced frequency can be evaluated and the Doppler shift is calculated. Therefore, the radial wind can be expressed by

$$V_R = \frac{\lambda}{2} \times \nu_D, \tag{1}$$

where λ is the wavelength of the transmitted laser and ν_D is the Doppler shift.

*Address all correspondence to: Zhifeng Shu, E-mail szf@ustc.edu.cn.

0091-3286/2014/$25.00 © 2014 SPIE

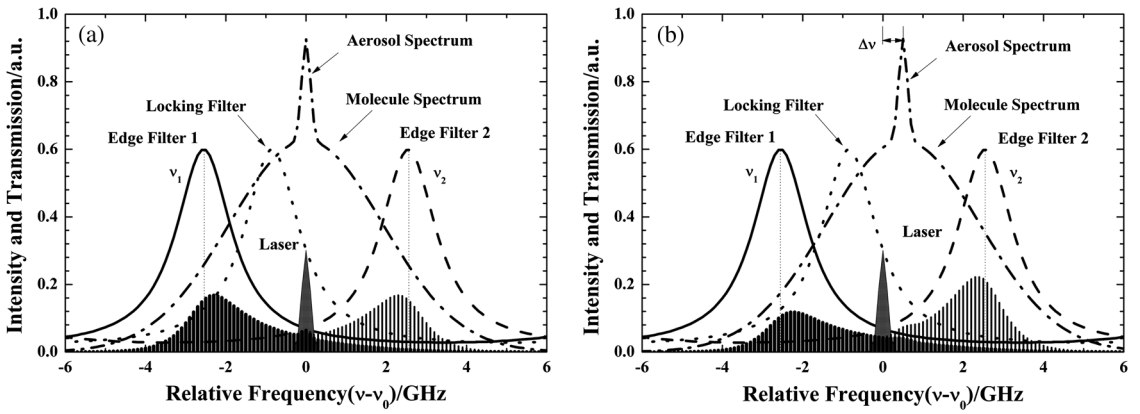

Fig. 1 Principle of double-edge technique for Rayleigh Doppler wind lidar (DWL) (a) for zero Doppler shift and (b) for 500 MHz Doppler shift.

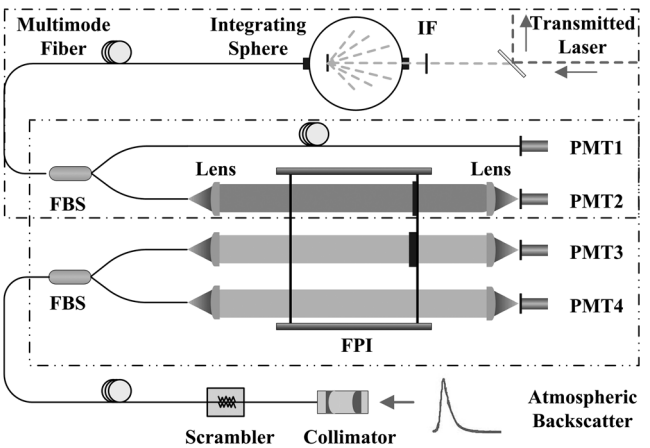

Fig. 2 Schematic setup of the optical receiver, IF: interference filter, FBS: fiber beam splitter, PMT: photomultiplier tube.

Table 1 Parameters of optical receiver.

Parameter	Value
FSR of FPI	12 GHz
FWHM of the edge	1.7 GHz
Edge separation	5.1 GHz
Locking separation	1.7 GHz
Peak transmission of FPI	60%
Quantum efficiency of PMT	>20%
Bandwidth of IF	0.15 nm
Fiber for locking	Core: 100 μm, NA.:0.22
Fiber for backscatter	Core: 200 μm, NA.:0.22
Diameter of IS	250 mm

Based on this principle of the measurement, a fiber-based optical receiver for direct detection lidar as is shown in Fig. 2 is designed. Two fiber beam splitters (FBSs) called locking channel FBS and signal channel FBS are applied in the system. The former, with a designed coupling rate of 20/80, guides a small portion of the transmitted laser split by a high reflectivity mirror for laser frequency locking, whereas the latter of 50/50 atmospheric backscatter. Then three parts are collimated through the triple-channel FPI and the fluxes are detected by photomultiplier tubes (PMTs) (Hamamatsu R7400). This PMT has a parallel analog and photon counting detection chain and an extended dynamic range. Considering the coupling efficiency of fiber, especially for atmospheric backscatter, the fiber type of the FBS is multimode. The scrambler is used after the collimator to make the distribution of the high order mode radiation uniform.[11] The parameters of the receiver are summarized in Table 1. Application of the integrating sphere (IS) will be discussed in Sec. 3.1.

2.2 *Laser Frequency Locking*

Before the wind observation, the instrument function of the FPI from which the frequency response function is derived, is measured by scanning the cavity length of the FPI. Theoretically, the transmission functions can be depicted in Fig. 3(a). However, during the process of wind measurement, the relative laser frequency to the FPI transmission functions will always vary, for example, such as the state illustrated in Fig. 3(b), due to the jitter and drift of the laser and dither of the FPI. This jitter of the laser and its measurement has been reported in Ref. 12. For the FPI, the noise equivalent displacement is $<10\ \mathrm{pm}\cdot\mathrm{Hz}^{1/2}$ and the temperature coefficient is <50 pm/K according to the specification offered by the manufacturer. A frequency bias would be introduced if these detected fluxes were applied to the calibrated sensitivity.

In order to prevent this relative frequency drifting out of the measuring range and maintain the accuracy of the measurement, the locking filter is applied to monitor the transmission of the laser. Meanwhile, an FPI controller adjusts the cavity length by changing the piezoelectric transducer voltage to drag the laser back to the zero position as in Fig. 3(a) according to the transmittance of the locking filter. Therefore, the laser transmission was first set at the half-magnitude point. During the wind measurement, the jitter and drift of laser and dither of the FPI would cause the departure of

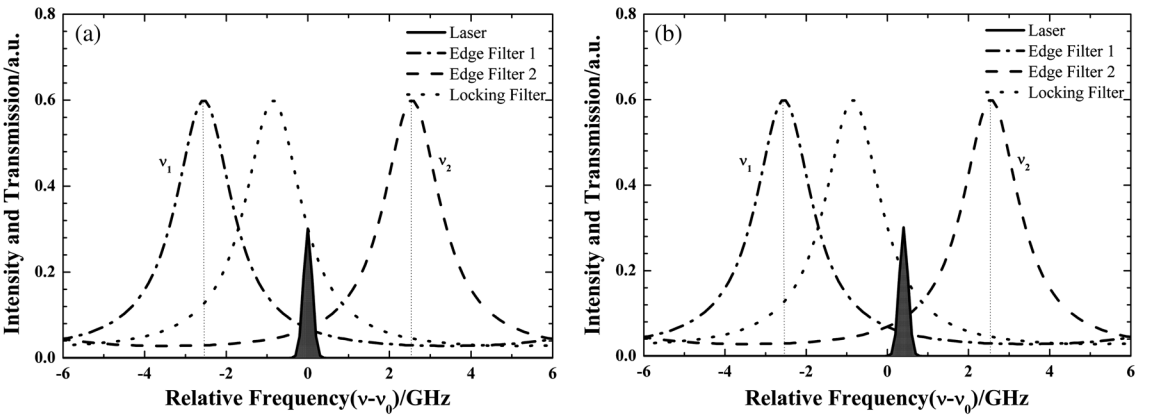

Fig. 3 Relative position between the transmitted laser and the FPI transmission function (a) no laser frequency shift, (b) laser frequency shift.

the set point and the servo-loop controller would tune the FPI appropriately according to the current transmission calculated from the response of the PMTs every 2 min, which is the same as our new DWL reported recently.[10]

2.3 *Accuracy Analysis of Frequency Locking*

The measured Doppler shift depends upon not only the accuracy retrieved from the edge channels but also on the locking channel. Beside the fact that a horizontal wind accuracy of 1 to 2 m/s (random error) should be ensured, the project in ESA[13] requires that the accuracy of the locking channel should be <1 m/s.

The triple-edge transmission function is an Airy function,[14] which is considered the angular divergence of the incident beam illuminated on the FPI, and can be expressed as follows:[7]

$$F_i(\nu) = \int_0^{\theta_{\max}} \frac{T_0 d\theta}{1 + 4\left(\frac{\mathrm{FSR}}{\pi\Delta\nu_{1/2}}\right)^2 \sin^2\left[\frac{2\pi\nu \cdot e_i \cos\theta}{c}\right]^2}, \qquad i = 1,2,L. \tag{2}$$

In this expression, "i" is 1, 2, and L which separately stand for edge filter 1, edge filter 2 and the locking filter, respectively. $\theta_{\max}$ is the angular divergence of the collimated beam (semiangle). T_0 is the peak transmission. The free spectral range (FSR) is the same for the three transmission function and the small difference between plates is several tens of nanometers, an $\sim 10^{-5}$ order of the cavity length, which does not affect the FSR. $\Delta\nu_{1/2}$ represents the full width at half magnitude (FWHM) of the function. e_i is the spacing gap for the corresponding filter. c is speed of light in vacuum.

We define the sensitivity of the locking filter from Eq. (2) as follows:

$$\Theta(\nu) = \frac{-1}{F_L(\nu)} \frac{dF_L(\nu)}{d\nu}. \tag{3}$$

As a result, the relative frequency shift is given as

$$\Delta\nu = \frac{F_L(\Delta\nu) - F_L(0)}{F_L(0)\Theta(\nu)}. \tag{4}$$

From Eqs. (1) and (4), the velocity bias caused by frequency jitter and drift and dither of the FPI is

$$v = \frac{\lambda}{2} \frac{F_L(\Delta\nu) - F_L(0)}{F_L(0)\Theta(\nu)}, \tag{5}$$

where $F_L(0)$ represents the transmittance when the relative frequency is zero or the locking frequency is the frequency of the laser. Due to the fact that the transmission function can be approximately linear around the locking area and the edge is steep with a slope value k of the order of 10^{-4} MHz^{-1}, Eq. (5) can be transferred to

$$v = \frac{\lambda}{2} \cdot \frac{-1}{k} [F_L(\nu) - F_L(0)], \tag{6}$$

where k is the slope of the transmission function and is considered to be a constant. Therefore, the measurement error is derived from Eq. (6) as

$$\delta v = \frac{\lambda}{2} \cdot \frac{-1}{k} \cdot \delta F_L(\nu). \tag{7}$$

For Rayleigh DWL, a laser with a wavelength of 355 nm is employed because of the Rayleigh backscatter coefficient dependence of λ^{-4} and thus a larger backscattering. k is a constant for a specific FPI, while $\delta F_L(\nu)$ depends on the measured transmittance of the locking channel. According to the locking process during wind measurement, F_L is calculated by

$$F_L(a_c) = a_c \cdot \frac{u_L}{u_E}, \tag{8}$$

where a_c is a calibrated constant, and u_L and u_E are the responses of the PMT in analogue mode, respectively. The relative frequency error is derived from Eqs. (7) and (8) as

$$\delta v = \frac{\lambda}{2} \cdot \frac{-1}{k} \cdot F_L(\nu) \cdot \frac{\delta a_c}{a_c}, \tag{9}$$

where we assumed that the responses of PMTs for u_L and u_E are sufficiently large and that $\delta u_L/u_L$ and $\delta u_E/u_E$ are both zero. Also, we define the $\delta a_c/a_c$ as the relative error of the calibrated constant. To minimize the error, two strategies may be used. One is improving the spectral resolution of

Table 2 Parameters of FPI for a typical Rayleigh DWL.

Parameter	Value
Spacing (FSR)	12.5 mm (12 GHz)
FWHM	1.7 GHz
Peak transmission	>60%
Reflectivity of plate at 355 nm	63.4%
Step of locking channel	25.15 nm
Locking channel separation	1.7 GHz
Step of filter two channels	75.44 nm
Edge channel separation	5.1 GHz

the locking channel. The other is measuring the calibrated constant with a high accuracy, especially for a fiber-based system.

Compared with Mie DWL, the spectrum of atmospheric backscatter is much wider for Rayleigh DWL. As a result, an FPI of low resolution is devised in the lidar system to ensure a higher sensitivity[14] for wind detection of the stratosphere and even higher altitudes.

However, this strategy only benefits the signal filters without consideration of the sensitivity while the same coating is applied to the locking filter. One thing should be noted; in our previous lidar system, the locking on the 1064-nm wavelength was chosen.[9] However, the consideration that any nonlinear process (e.g., second- and third-harmonic generation) may result in displaced or distorted spectra changes our decision. The wavelength of the transmitted laser, 355 nm, was chosen for the locking. A typical FPI design is illustrated in Table 2 and the corresponding slope of the locking

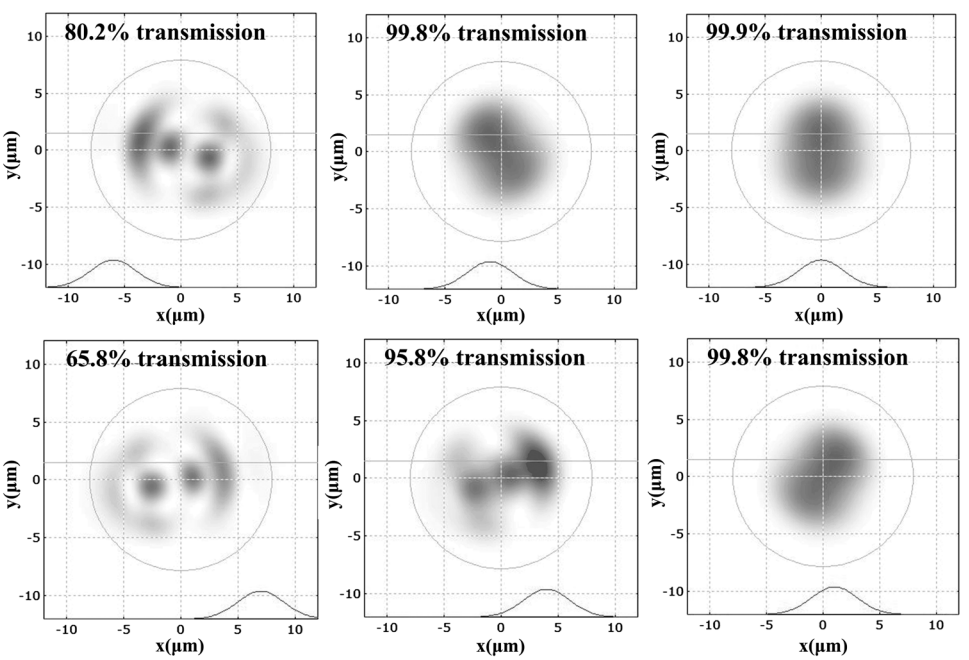

Fig. 4 Mode distributions and transmissions for different beam locations on a multimode fiber.

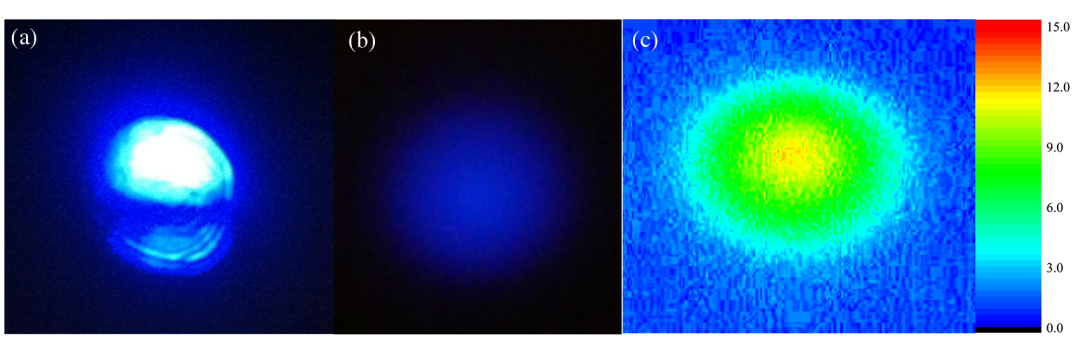

Fig. 5 Laser pattern (a) before integrating sphere (IS) and (b) after IS, and (c) represents the distribution of the laser pattern in (b).

transmission is 3.5×10^{-4} MHz^{-1}. Then the required relative error of the calibrated constant must be <0.66% for the requirement of a velocity error of 1 m/s according to Eq. (9). To guarantee the locking accuracy, efforts should be taken to increase the accuracy of the calibrated constant, decrease the relative error of the calibrated constant and increase the slope of the transmission function.

3 Improvements

3.1 *Measurement of Calibrated Constant with High Accuracy*

As depicted in Fig. 2, a multimode FBS is applied for relative laser frequency monitoring. Compared with a single-mode fiber, multimode fibers not only have a significantly larger core area but also a generally higher numerical aperture. These characters make launching free-space light into a multimode fiber comparatively easy with a high efficiency because of the large tolerances concerning the location and the angle of the incident light.[15]

However, the optical electric field distribution in a multimode fiber is a superposition of contributions from different modes, the intensity profile depends upon the optical powers in all the modes, and there can be constructive or destructive interference of different modes at a particular location in the fiber. The power distribution and transmission are initially determined by the beam location, as illustrated in Fig. 4, and the incident angle. Also, bending of the fiber and changes of the wavelength or temperature will modify the power distribution.[16]

For a multimode FBS, the specific power distribution, which means the specific modes contribution, will cause a specific coupling rate. Therefore, while launching free-space light to multimode FBS in a general way, for instance, with a lens, the coupling rate will mainly change for two reasons. One is the distribution of the input light while the other is the incident angle. This unpredictable variance of the coupling rate will cause a large $\delta a_c/a_c$ in Eq. (9), and thus a large laser frequency locking error.

To decrease these two kinds of interference, the IS is deployed in the optical receiver as illustrated in Fig. 2. The laser beam transmits into the IS via free path and the uniform scatter illuminates the little hole where the fiber end is placed. An alternative application utilizes the port opening of an internally illuminated IS as a large area source that features uniform radiance.[17] The relative theory of IS is described elsewhere.[18,19]

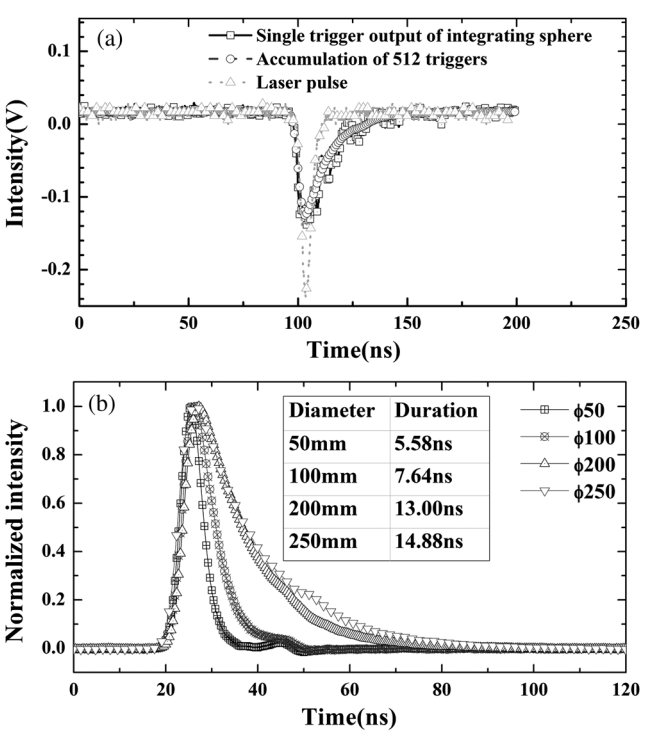

Fig. 6 (a) Laser widened by an IS with a diameter of 200 mm, (b) pulses widened by IS of different radii. The incident laser is from Continuum Powerlite 9030 with pulse duration of 5 ns.

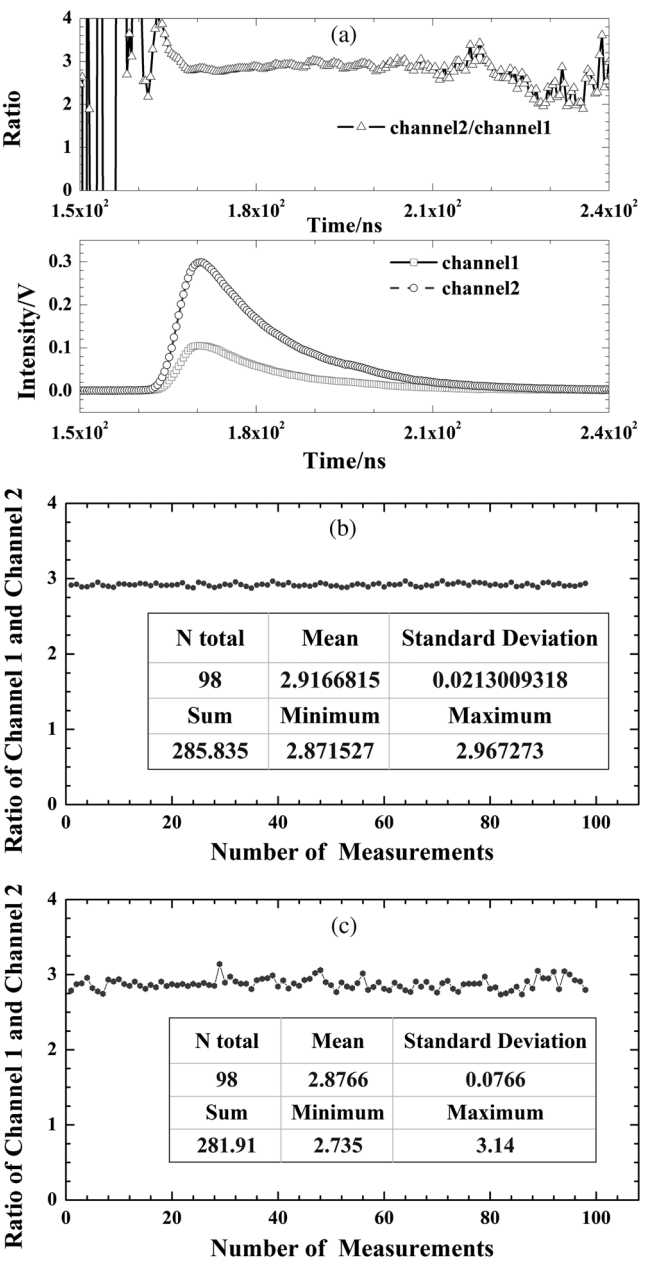

Fig. 7 (a) Typical waveforms response of PMTs for calibrated constant measurement and its ratio with IS, (b) and statistical result of 98 measurements. (c) Measurements without IS.

In this receiver, the feature of uniform scattering or a diffusing effect for IS is applied. The laser, usually with complicated patterns [in Fig. 5(a)] for a flash-pumped and frequency-tripled Nd:YAG laser because of diffraction and interference or other reasons, is internally scattered and diffused with a uniform output pattern as shown in Fig. 5(b). The blue pattern is the fluorescence of the frequency-tripled Nd:YAG laser when exposured to white paper.

Another advantage for applying IS is that the short pulse will be temporally widened. This pulse widening feature is illustrated in Fig 6(a). The laser entered into the IS with a diameter of 200 mm. The negative pulse depends on the design of the PMT. The output pulses with a single trigger (solid) and an accumulation of 512 triggers (dash) are widened with a duration of about 13 ns. Compared with the response of the incident pulse, the outgoing pulse was widened.

We also measured the outgoing pulse from ISs of different diameters. The duration of the output pulse is dependent on the diameter of the sphere, as shown in Fig. 6(b). This measurement of the pulse duration revealed that the pulse duration is positively dependent on the IS diameter. With this special feature, more samples will be collected for the same analog-to-digital (AD) card and the measurement error will decrease.

Utilizing the above uniform resource and duration-widened pulse, the calibrated constant is measured. The experimental setup can also be illustrated in the dash dot frame in Fig. 2. The IS with a diameter of 250 mm is applied in the experiment. During the process, the FPI is removed and the output signals of the PMTs are acquired by an oscilloscope (Tektronix DPO3034).

The results are presented in Fig. 7. Theoretically, the two waveforms responding from the PMT1 and PMT2 are similar and the only difference is the magnitude. Therefore, the ratios of the corresponding points between these waveforms are constant. However, there are points which vary quickly or around zero due to a low signal-to-noise ratio. The ratios oscillate in these areas as is illustrated in Fig. 7(a). During data processing, points with a huge deviation will be removed due to the above reasons. Therefore, it is reasonable to take advantage of the points which fall in the FWHM area for the calculation. The ratios of the corresponding points in the area are averaged and the result is the measured calibrated constant. 98 waveforms of the same measurement were continuously acquired and the results are presented in Fig. 7(b) with the statistical outcome in the table. The same measurements without IS were achieved and the results are presented in Fig. 7(c). The relative error of the calibrated constant with IS is 0.72%, which is a relatively stable result compared with the results of 2.66% without IS.

With IS applied in the lidar system, wind observation was carried out at Delhi (37.371° N, 97.374° E) in Qianghai province of China in December 2013. The system description can be found in detail in Ref. 10. A half hour accumulation of backscatter for each wind profile was selected to abate the statistical error of measurements, with a spatial resolution of 200 m below 40 km and extending to 1000 m beyond 40 km. Wind detection by radiosonde is also simultaneously available near the observation location. A typical wind measurement result of our lidar (circle) is presented in Fig. 8 with the wind detection result using a balloon (square). Comparison between the results of these two techniques demonstrates a good agreement <30 km while radiosonde data is not available >30 km.

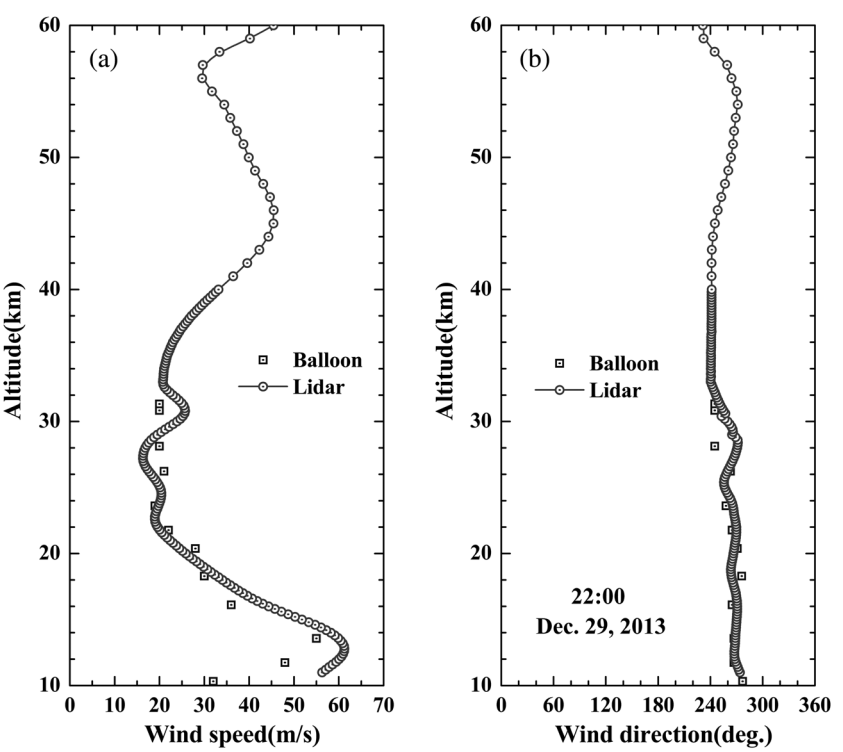

Fig. 8 Typical profile of (a) wind speed and (b) wind direction observed by lidar and balloon at Delhi in Qianhai province.

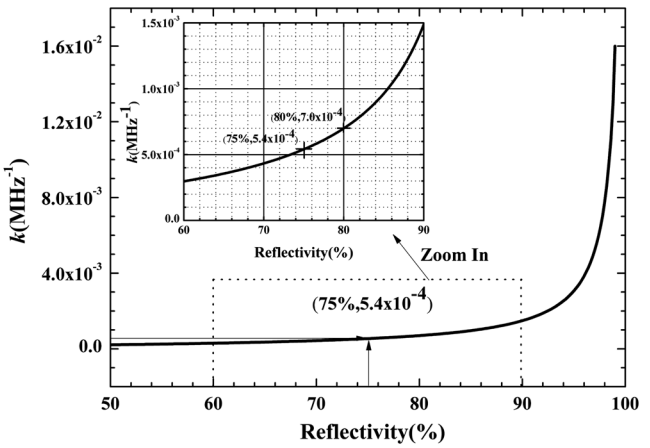

Fig. 9 Slope of transmission function dependence on the reflectivity of the FPI.

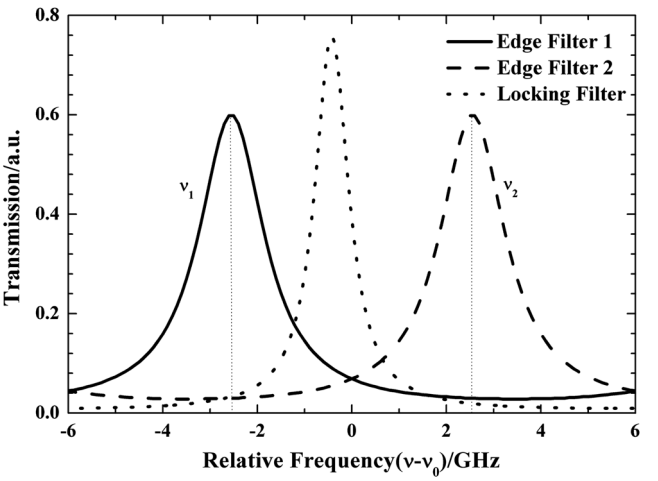

Fig. 10 Transmission function of the triple-edge channels for the optimized FPI.

3.2 *Improvement for FPI*

From Sec. 3.1, the calibrated constant is measured with a high accuracy by applying the IS. However, the relative error is higher than the value of 0.66% calculated in Sec. 2.3 using the current FPI with the requirement of the locking frequency error. Therefore, improvement should be proposed to increase k in Eq. (9) for locking filter.

According to the transmission function in Eq. (2), we can determine the transmission function dependence of the reflectivity of plates as

$$F_L(\nu,R)=\int_0^{\theta_{\max}}\frac{T_0 d\theta}{1+4\left(\frac{\sqrt{R}}{1-R}\right)^2\sin^2\left[\frac{\pi\left[\nu+\frac{\mathrm{FSR}\cdot(1-R)}{2\pi\sqrt{R}}\right]\cos\theta}{\mathrm{FSR}}\right]^2}, \quad (10)$$

where the equation $\frac{\mathrm{FSR}}{\Delta\nu_{1/2}}=\frac{\pi\sqrt{R}}{1-R}$ and $\mathrm{FSR}=\frac{c}{2L}$ are applied. R represents the reflectivity of the plates. Figure 9 shows the transmission dependence of R with the assumption that the half magnitude point in the falling edge is zero for the maximum sensitivity in this area. The slope increases while increasing the reflectivity of the plates.

With an extended measurement error of the calibrated constant to 1% combined with the frequency locking requirement, the slope of the locking filter transmission function should be larger than 5.4×10^{-4} MHz^{-1} according to Eq. (9). The slope of the transmission function for the locking filter dependence on reflectivity is shown in Fig. 8. It can be concluded that a reflectivity larger than 75% at 355 nm will meet the error requirement and the larger, the better. However, considering the tradeoff between the coating cost and the accuracy requirements, we select the reflectivity of 80% at a wavelength of 355 nm with a k of 7.0×10^{-4} MHz^{-1}. The new FPI parameters are given in Table 3.

Based on this design of the FPI, the triple-edge transmission functions are calculated and shown in Fig. 10. The reflectivity of the new coating for the locking filter results in a narrower FWHM of about 854 MHz. With the measured calibrated constant, the relative laser locking frequency error is about 11 MHz without IS, while it is about 3 MHz with IS, which means a radial velocity of 0.53 m/s.

Table 3 The parameters of the optimized FPI for laser frequency locking.

Parameter	Value
Spacing (FSR)	12.5 mm (12 GHz)
Peak transmission	>60%
Reflectivity of plate at 355 nm (Locking filter excluded)	63.4%
FWHM of edge channel	1.7 GHz
Reflectivity of plate at 355 nm (locking filter)	80.0%
FWHM of locking channel	0.854 GHz
Step of locking channel	31.40 nm
Locking channel separation	2.1 GHz
Step of filter two channels	75.44 nm
Edge channel separation	5.1 GHz

4 Summary and Conclusion

A fiber-based optical receiver for direct detection DWL was designed. Specifically, the locking error of the relative laser frequency was analyzed. It turns out that the locking error is dependent on the relative error of the calibrated constant and the slope of the transmission function. The relative error of the calibrated constant lies in the fact that the distribution and the angle of the incident light would alter the distribution of the guided modes in a multimode FBS and thus the coupling rate of the FBS, while the latter the low spectral resolution of the locking filter of FPI.

According to the analysis, two strategies were employed. First, the IS was applied to couple the free-space light into the fiber for its characteristic of uniform scattering. An extra feature of widening of the pulse duration results in more samples being acquired for the AD card of the same sampling rate. Thus, a measurement of higher accuracy is achieved with a relative error of 0.72% for the calibrated

constant. Second, the new locking channel of the FPI is designed with a higher reflectivity of 80% at 355 nm. With these improvements, the frequency error of the locking channel is evaluated and is about 3 MHz, which suggests that the radial velocity error of 0.53 m/s is caused by the locking filter.

Acknowledgments

The author is appreciative for the discussion on FPI with Dr. C. Pietraszewski from IC Optical Systems Ltd. This work was supported by National Natural Science Foundation of China (41174130, 41174131, 41274151, 41304123) and the Fundamental Research Funds for the Central Universities (WK2080000048).

References

1. J. W. Meriwether and A. J. Gerrard, "Mesosphere inversion layers and stratosphere temperature enhancements," *Rev. Geophys.* **42**, RG3003 (2004).
2. B. M. Gentry, H. Chen, and S. X. Li, "Wind measurements with 355-nm molecular Doppler lidar," *Opt. Lett.* **25**, 1231–1233 (2000).
3. O. Reitebuch et al., "The airborne demonstrator for the direct-detection Doppler wind lidar ALADIN on ADM-Aeolus: I. Instrument design and comparison to satellite instrument," *J. Atmos. Ocean. Tech.* **26**, 2501–2515 (2009).
4. W. Baker et al., "Lidar-measured wind profiles: the missing link in the global observing system," *Bull. Am. Meteorol. Soc.* **95**, 543–564 (2014).
5. C. L. Korb et al., "Theory of the double-edge technique for Doppler lidar wind measurement," *Appl. Opt.* **37**, 3097–3104 (1998).
6. C. Flesia and C. L. Korb, "Theory of the double-edge molecular technique for Doppler lidar wind measurement," *Appl. Opt.* **38**, 432–440 (1999).
7. C. Souprayen, A. Garnier, and A. Hertzog, "Rayleigh–Mie Doppler wind lidar for atmospheric measurements. II. Mie scattering effect, theory, and calibration," *Appl. Opt.* **38**, 2422–2431 (1999).
8. Z. Shu et al., "Low stratospheric wind measurement using mobile Rayleigh Doppler wind LIDAR," *J. Opt. Soc. Korea* **16**, 141–144 (2012).
9. H. Xia et al., "Mid-altitude wind measurements with mobile Rayleigh Doppler lidar incorporating system-level optical frequency control method," *Opt. Express* **20**, 15286–15300 (2012).
10. X. Dou et al., "Mobile Rayleigh Doppler Lidar for wind an temperature measurements in the stratosphere and lower mesosphere," *Opt. Express* **22**, A1203–A1221 (2014).
11. H. Xia et al., "Fabry–Perot interferometer based Mie Doppler lidar for low Tropospheric wind observation," *Appl. Opt.* **46**, 7120–7131 (2007).
12. T. Schröder et al., "Frequency jitter and spectral width of an injection-seeded Q-switched Nd:YAG laser for a Doppler wind lidar," *Appl. Phys. B* **87**, 437–444 (2007).].
13. European Space Agency (2008), *ADM-Aeolus Science Report*. ESA SP-1311, 45 (2008).
14. C. L. Korb, B. M. Gentry, and C. Y. Weng, "Edge technique: theory and application to the lidar measurement of atmospheric wind," *Appl. Opt.* **31**, 4202–4213 (1992).
15. F. Mitschke, *Fiber Optics: Physics and Technology*, Springer, Berlin (2009).
16. R. Paschotta, "RP Photonics Encyclopedia for Multimode Fibers," http://www.rp-photonics.com/multimode_fibers.html (October 2008).
17. K. F. Carr, "Integrating sphere theory and applications Part II: integrating sphere applications," *Surf. Coat. Int.* **80**, 485–490 (1997).
18. D. G. Goebel, "generalized integrating sphere theory," *Appl. Opt.* **6**, 125–128 (1967).
19. K. F. Carr, "Integrating sphere theory and applications. Part I: integrating sphere theory and design," *Surf. Coat. Int.* **80**, 380–385 (1997).

Feifei Zhang received his MS degree in the Key Laboratory of Atmospheric Composition and Optical Radiation, Anhui Institute of Optics and Fine Mechanics, CAS, in 2012 and his BS degree in the School of Science, Northwest Polytechnical University, in 2009. Now he is a doctoral student at the University of Science and Technology of China, and his technical research is mainly focused on Doppler wind lidar.

Xiankang Dou is a professor at the University of Science and Technology of China. His current research field includes stratosphere, mesosphere, and lower thermosphere (SMLT) dynamics and waves, laser remote sensing technology and lidar atmospheric sensing.

Dongsong Sun is a professor at the University of Science and Technology of China. His current research interests include lidar technology, lidar remote sensing, and Doppler wind lidar technology.

Zhifeng Shu received his BS degree in physics from China University of Petroleum in 2007. He received MS degree and PhD degrees in optics from Anhui Institute of Optics and Fine Mechanics, Chinese Academy of Sciences, in 2009 and 2012, respectively. Upon graduation, he joined the University of Science and Technology of China as a postdoctoral. His current research interests include all-optical signal processing, photodetection, and laser remote sensing.

Haiyun Xia received his BS degree in physics and his MS degree in optics from Soochow University in 2003 and 2006, respectively. In 2010, he received his PhD degree in optoelectronics from the University of Ottawa and Beijing University of Aeronautics and Astronautics. He joined the University of Science and Technology of China in 2011 as an associate professor. His current research interests include Doppler wind lidar, femtosecond laser pulse characterization, and applications and fiber-optic sensors.

Yuanyuan Gao received her BS degree in physics from Hefei Normal University in 2012. She is pursuing her MS degree at the University of Science and Technology of China. Her current research interests include data analysis of Doppler wind lidar.

Dongdong Hu received his BS degree in microelectronics from Hefei University of Technology in 2008 and his MS degree in optics from Anhui Institute of Optics and Fine Mechanics, Chinese Academy of Science, in 2011. He is pursuing his PhD at the University of Science and Technology of China. His current research interests include fiber application in laser remote sensing and photon detection.

Mingjia Shangguan received his BS degree from Jilin University of Architecture in 2012. He is pursuing his MS degree at the University of Science and Technology of China. His current research interests include the atmospheric Rayleigh-Brillouin scattering and signal processing.